Silicon (2017) 9:285–291
DOI 10.1007/s12633-015-9356-x

ORIGINAL PAPER

Optical and Structure Properties of Nanocrystalline Titania Powders with Cu Dopant

Nasrollah Najibi Ilkhechi[1] · **Behzad Koozegar Kaleji**[1]

Received: 8 December 2014 / Accepted: 11 September 2015 / Published online: 5 January 2016

Abstract TiO_2 nanopowders doped by Cu were prepared by the sol–gel method. The effects of Cu doping on the structural, optical, and photo-catalytic properties of titania nanopowders have been studied by X-ray diffraction (XRD), scanning electron microscopy (SEM), transmission electron microscopy (TEM), and UV–Vis absorption spectroscopy. XRD results suggest that adding impurities has a significant effect on anatase phase stability, crystallinity, and particle size of TiO_2. Titania rutile phase formation in the system (Ti–Cu) was promoted by Cu^{2+} doped TiO_2. The photo-catalytic activity was evaluated by photo-catalytic degradation kinetics of aqueous methylene orange (MO) under visible radiation. The results show that the photo-catalytic activity of the 5 %Cu doped TiO_2 nanopowders has a larger degradation efficiency than pure TiO_2 under visible light. Also, the minimum band gap was estimated to be ~ 1.9–2 eV from UV–Vis spectra.

Keywords TiO_2 nanocomposite · Sol–gel · Cu dopant · Optical properties

1 Introduction

Titania (TiO_2) crystallizes in three phases: brookite (rhombohedral, a = 5.43 Å; b = 9.16 Å; c = 5.13 Å), anatase (tetragonal, a = b= 3.78 Å; c = 9.50 Å), and rutile (tetragonal a = b= 4.58 Å; c = 2.95 Å). The brookite and anatase crystalline phases, which are stable at lowtemperatures, transform into rutile by calcination at higher temperatures. However, brookite and anatase can be stabilized at high temperatures in the presence of dopants during synthesis which inhibits their transformation into rutile [1–4]. Among various phases of titania, anatase shows better photocatalytic activity with anti-bacterial performance [5–9]. A stable anatase phase up to the sintering temperature of the ceramic substrates is the most desirable property for applications of anti-bacterial self cleaning building materials (e.g., bathroom tile, sanitary wares, etc.) These applications require high purity titania with a definite phase composition [10–12].

TiO_2 doped with Ce, V, Cu, Sn, Nd, Fe, Cr or Co shows a red shift of the absorption band compared to pure TiO_2, and considerable photocatalytic activity under visible light Irradiation [13–19]. Sensitization of Cu doped TiO_2 with eosin improved the photocatalytic activity for water splitting under visible light irradiation [15]. In this case, CuO not only brings about the charge separation but also provides active sites for water splitting. Some recent studies have revealed that the oxygen deficient sites play a crucial role in the visible light induced photocatalytic activity of TiO_2. Ihara et al. [20] have reported that the low temperature H_2 plasma treated TiO_2 and nitrogen doped TiO_2 [21] showed visible light photocatalytic activity due to the presence of oxygen deficient sites.

Prokes et al. [22] have proposed that the visible light absorption of titanium oxynitride is due to the oxygen hole center created during the surface modification process by nitrogen near the surface of the nano-colloid. The visible light photocatalytic activity observed due to the oxygen

✉ Nasrollah Najibi Ilkhechi
nasernajibi@gmail.com

Behzad Koozegar Kaleji
b.kaleji@malayeru.ac.ir

[1] Department of Materials Engineering, Faculty of Engineering, Malayer University, P.O. Box: 65719-95863, Malayer, Iran

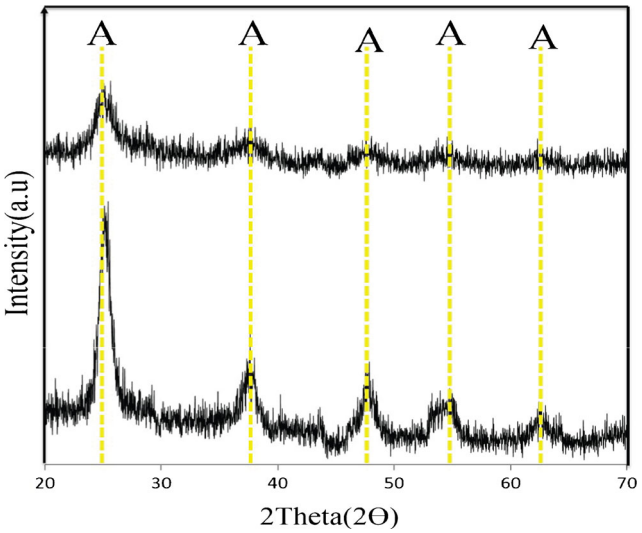

Fig. 1 XRD spectra of the pure and doped TiO_2 nanopowders at 500°C **a** TiO_2 (T), **b** TiO_2-5 %Cu (TC)

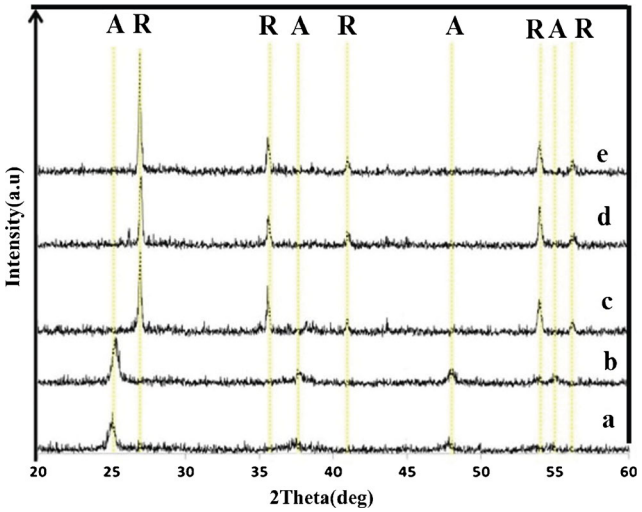

Fig. 2 XRD spectra of the T-5 %Cu (TC) nanopowders at different temperatures **a** 600°C, **b** 700°C, **c** 800°C, **d** 900°C, **e** 1000°C

vacancies in TiO_2 is found to decrease after an optimum value.

In this paper, TiO_2 nanopowders doped by Cu were prepared by the sol–gel method. The effect of the dopant cations on the stability of the anatase phase and optical properties at high temperature was studied. The efficiency of these samples as photocatalysts for degradation of MO, as an organic compound model, under visible light was investigated.

2 Experimental Procedures

2.1 Preparation of the Doped Titania Nanopowders

The preparation of the precursor solution for Cu doped TiO_2 nanopowder is as follows: TiO_2 and CuO sols were prepared separately. Titanium (IV) butoxide (TBT = $Ti(OC_4H_9)_4$, Aldrich) was selected as the titanium source. 10 ml of ethanol (EtOH, Merck) and 4 ml of ethyl acetoacetate, which is a sol stabilizer, were mixed, and then 4 ml of TBT was added at the rate of 1 ml/min to the mixture at ambient temperature (25^0C). The solution was continuously stirred for 1 h, followed by dropping of HNO_3 as catalyst to the solution. Deionized water was added into the solution slowly to initiate the hydrolysis process. The solution was aged for 24 h in order to complete all reactions. The chemical composition of the alkoxide solution was TBT: H_2O: HNO_3: EAcAc: EtOH = 1: 8: 3: 0.05: 5 in volume ratio. In order to prepare the CuO sol, $Cu(NO_3)_2.3H_2O$ (Merck) was dissolved in EtOH with a volume ratio of $Cu(NO_3)_2.3H_2O$: EtOH = 1:6 at ambient temperature with continuous stirring. Cu was doped under continuous stirring at room temperature for 40 min. The formed gel was dried at 100°C for 60 min. Finally, the prepared samples were calcined at desired temperatures (500, 600, 700, 800, 900, 1000°C) for 2 h.

2.2 Characterization Methods

Samples were studied using X-ray diffraction analysis (Philips, MPD-XPERT, λ:Cu K_α = 0.154 nm). The samples were scanned in the 2θ range of 20°–60°. The average crystallite size of nanopowders (d) was determined from the XRD patterns, according to the Scherrer equation (1) [23]

$$d = k\lambda/\beta\cos\theta \quad (1)$$

where k is a constant (shape factor, about 0.9), λ the X-ray wavelength (0.154 nm), β the full width at half maximum (FWHM) of the diffraction peak, and θ is the diffrac-

Table 1 Characterization of pure and doped TiO_2(TC) at temperature 500^0C

Sample	Å %	R %	Crystallite Size(nm)		a = b (Å)	c (Å)	Cell Volume $(Å)^3$	S m^2/g
			d_A	d_R				
TiO_2(T)	100	–	9.47	–	3.767	8.944	126.917	183.2
T-5 %Cu (TC)	100	–	8.35	–	3.798	12.086	174.331	208.7

Table 2 Characterization of 5 % Cu doped TiO_2(TC) at different temperature

Calcination temperature	Å %	R %	Crystallite Size(nm)		a=b (Å)	c (Å)	Cell Volume(Å)^3	S m^2/g
			d_A	d_R				
600^0C	100	-	10.19	-	3.796	9.431	136.009	150.9
700^0C	100	-	13.89	-	3.770	6.019	85.547	110.7
800^0C	-	100	-	17.93	4.679	2.997	65.613	79.6
900^0C	-	100	-	24.50	4.681	2.991	65.538	58.3
1000^0C	-	100	-	32.36	4.664	3.000	65.258	44.1

tion angle. The values of β and θ of anatase and rutile phases were taken from anatase (101) and rutile (110) planes diffraction lines, respectively. The amount of rutile in the samples was calculated using the following equation (2) [23]

$$X_R = (1 + 0.8(I_A/I_R))^{-1} \quad (2)$$

where X_R is the mass fraction of rutile in the samples, and I_A and I_R are the X-ray integrated intensities of the (101) reflection of the anatase and (110) reflection of rutile, respectively. The diffraction peaks of crystal planes (101), (200), and (105) of the anatase phase in XRD patterns were selected to determine the lattice parameters of the TiO_2 and doped TiO_2 nanopowders. The lattice parameters were obtained by using Eq. 3 [23]

$$(Bragg's\ law) : 2d_{(hkl)}sin\theta = \lambda$$

$$(1/d_{hkl})^2 = (h/a)^2 + (k/b)^2 + (l/c)^2$$

where $d_{(hkl)}$ is the distance between the crystal planes of (h k l); λ is the wavelength of X-ray used in the experiment; θ is the diffraction angle of the crystal plane (h k l); h k l is the crystal plane index; and a, b, and c are lattice parameters (in anatase form, a = b ≠c).

The morphology of the nanopowder was observed using a scanning electron microscope (SEM, XL30 Series) with an accelerating voltage of 10–30 kV. TEM imaging was carried out using a Zeiss-EM10C-80 kV instrument. FTIR absorption spectra were obtained over the range of 4000–400 cm^{-1} at room temperature.

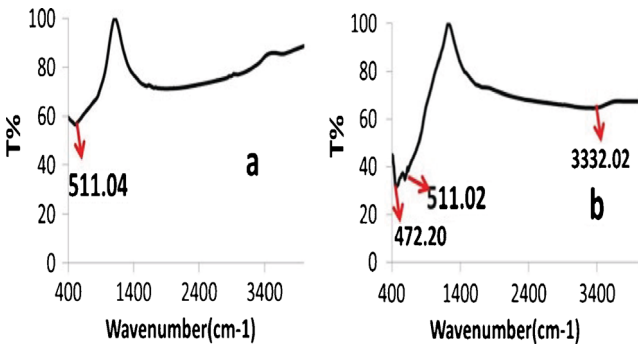

Fig. 3 FTIR spectra of pure and doped TiO_2 nanoparticles calcined at temperatures 500°C **a** T, **b** TC

2.3 Photo-catalytic Activity Measurement

The photocatalytic activity was evaluated by monitoring the degradation of MO solution under visible illumination. In each experiment, 0.08 g standard sample calcined at different temperatures was dispersed in 50 mL of MO solutions with concentration 5×10^{-6} M. Visible irradiation was provided by a xenon lamp (500 W) equipped with a cutoff filter to remove light with wavelength below 400 nm. Before the test, all powders containing MO solutions were magnetically stirred in the dark for 1 h to establish adsorption–desorption equilibrium. Then, the solutions were irradiated under visible light with a constant stirring rate of 450 rpm. After 40 min irradiation, 5 ml of supernatants were taken from the suspension by a syringe filter unit to scan the UV–vis absorption spectrum. The UV–vis absorption spectra of samples were measured between 200 and 1000 nm. The extent of the methyl orange decomposition was determined by measuring the value of the absorbance value at 478 nm (max absorption of MO) using a UV–vis spectrometer. The degradation rate (η (%)) of methyl orange was calculated by the following formula: where A_0 and A_t represent the initial equilibrium concentration and reaction concentration of the reactant at 478 nm, respectively (3) [23].

$$\eta(\%) = (A_0 - A_t)/A_0 \times 100 \quad (3)$$

3 Results and Discussion

3.1 X-ray Diffraction Studies of the Nanopowders

Figure 1 shows the XRD patterns of pure and doped TiO_2 nanopowders with 5 % mol of Cu heat treated at 500 °C for 2 h. The X-ray diffraction peak at 25.3° corresponds to the characteristic peak of the crystal plane (101) of anatase. According to XRD patterns, the pure and doped TiO_2 (T) consisted of pure anatase phase. No characteristic peaks of

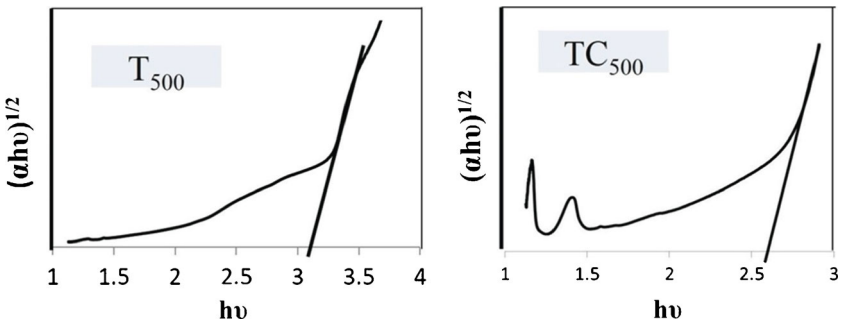

Fig. 4 Tauc plots of T, T–5 %Cu (TC) nanopowders calcined at 500^0C

CuO were observed in doped TiO_2 nanopowders which suggests the incorporation of Cu^{2+} into the TiO_2 lattice [24, 25]. The calculated crystallite sizes of anatase, calculated by the Scherrer formula, are given in Table 1. The decrease in crystal size can be attributed to the presence of Cu-O-Ti in the doped TiO_2 nanopowders, which inhibits the growth of crystal grains. According to Table 1, the crystallite size and surface area of pure and doped TiO_2 nanopowders at a temperature of 500°C is as follows: d_T (nm) > d_{TC} (nm), S_T (m^2/g) < S_{TC} (m^2/g).

The XRD patterns of 5 % mol of Cu doped TiO_2, nanopowders calcined at different temperatures are shown in Fig. 2. Samples heated at 500 − 700°C show only the anatase phase and at 800 − 1000°C the samples show the rutile phase. The addition of Cu has a promoting effect on the transformation of anatase to rutile crystalline phase [25, 26]. All the samples were identified as the mixture polymorphs of anatase or rutile without any impurity phase. The ionic radius of the Cu^{2+} ion (CN: 4, 0.58Å) approaches that of the Ti^{4+} ion (CN: 6, 0.66Å) in TiO_2 and the Cu^{2+} ions will replace lattice Ti^{4+} ions and thus occupy lattice Ti^{4+} positions in the doping reactive process. It is clear from Table 2 that the crystallite size increased but the surface area decreased with increase of the calcinations temperature for anatase (600°C, 700°C) and rutile (800 − 1000°C) nanoparticles.

3.2 FTIR Analysis of Pure and Doped TiO_2 nanopowders

Figure 3 shows the FTIR spectrum of the nanocrystalline TiO_2 powder calcined at temperature 500°C in the range of 400-4000 cm^{-1} Metal oxides generally give absorption

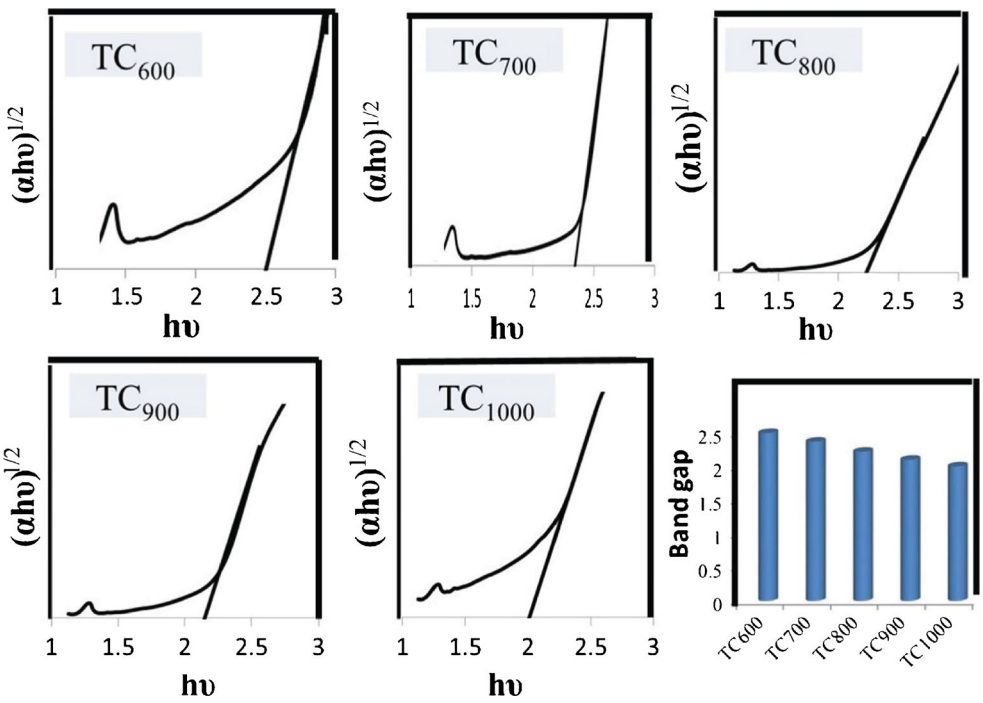

Fig. 5 Tauc plots of Cu doped TiO_2 nanoparticles at different temperatures

bands in the finger print region below 1000 cm^{-1} arising from inter-atomic vibrations. The infrared spectra (Fig. 3) of pure and doped TiO_2 exhibits the following bands:

(i) 3332.02 cm^{-1} due to intermolecular structure and the O–H band [27]
(ii) 511.02 cm^{-1} and 511.04 cm^{-1} which can be attributed to the Ti-O stretching and Ti-O-Ti binding stretching modes [28].
(iii) 472.02 cm^{-1} which can be attributed to the vibrations of Cu–O [29].

3.3 Photocatalytic Evaluation

The optical band gap (E_g) is calculated using the UV–vis spectra by [29]:

$$\alpha h\upsilon = A(h\upsilon - E_g)^n \quad (4)$$

where $h\upsilon$ is the photon energy, A and n are constants. For allowed direct transition n = 1/2, direct forbidden transition n = 3/2 and indirect allowed transition n = 2.The optical band gap energy (E_g) is found by extrapolating the straight line portion of $(\alpha h\upsilon)^{1/2}$ with the abscissa axis ($h\upsilon$) in the vicinity of the fundamental optical transition for pure and doped nanopowders. It can be seen from Tauc plots (Fig. 4) that the band gap of pure TiO_2 nanoparticles is 3.12 eV. Also, the values of the band gap calculated from Tauc plots are found to be 2.65 for TC at temperature 500°C. It indicates a decrease in the energy band gap for Cu doped samples (inset in Fig. 4). It has been reported that metal doping could form a dopant energy level within the band gap of TiO_2 [30, 31].

The UV-Vis DRS of TC calcined at 600°C- 1000°C are illustrated in Fig. 5, which shows that the band gap of samples decreased with the increase of the calcination temperature. The largest reduction band gap is observed for 5 % mol of Cu doped TiO_2 at temperature 1000°C (2 ev). This large reduction band gap may be attributed to those impurities incorporated into the host (TiO_2) structure which create extra energy levels within the band gap. When the calcination temperature is below 700°C, the red-shift of the absorption edge wavelength can be attributed to the growth of TiO_2 crystallites. At 800°C −1000°C, the red-shift is due to the increased crystallite size and phase transformation from anatase to rutile, leading to the decrease of band gap energy.

Figure 6 shows the results of photo-catalytic decomposition of MO solution caused by degradation of MO in contact with nanopowders with Cu dopant at different calcination temperatures. According to Fig. 6, the order of photocatalytic activity of TiO_2 nanopowders at 40 min under the visible irradiation is TC > T, which suggests that the doping enhances the photo-catalytic activity of TiO_2. This enhanced photocatalytic activity is because of suppressed recombination of photogenerated electrons and holes.

Figure 6 shows that nearly 72 % of MO was decomposed in the presence of T-5 %Cu after visible irradiation for 40 min. When Cu is introduced to TiO_2 nanopowders, the TiO_2 nanocomposite are different from pure TiO_2 nanopowders

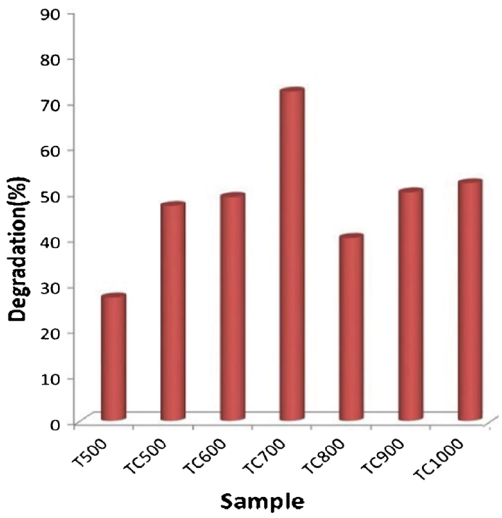

Fig. 6 Photocatalytic degradation of MO determined by pure and doped TiO_2 nanopowders after 40 min visible irradiation at different temperature

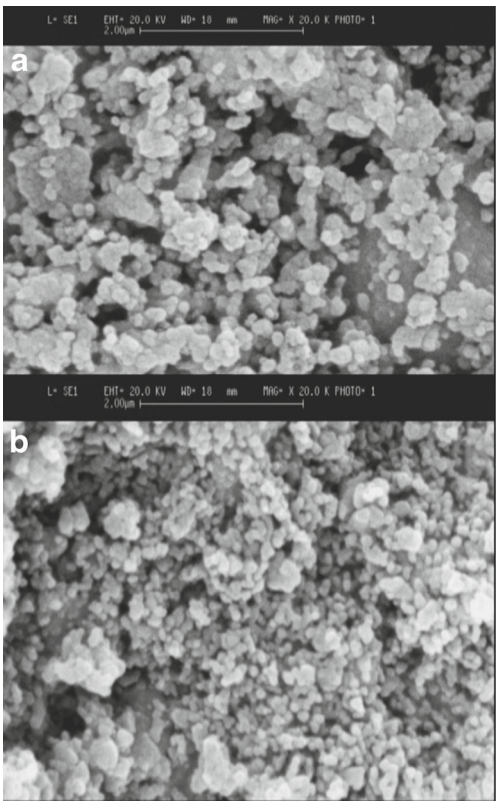

Fig. 7 SEM images of pure and doped TiO_2(TC)nanopowders calcinations at 500 °C **a** T, **b** TC

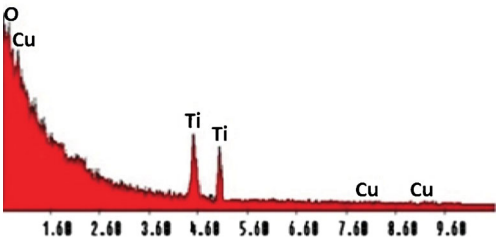

Fig. 8 EDX images of doped TiO_2(TC)nanopowders calcinations at 500 °C

in both physical and chemical characteristics, such as phase types (Figs. 1 and 2), surface areas, crystallite size (Tables 1 and 2), and chemical compositions. An optimum calcination temperature of doped TiO_2 shows higher activity than pure TiO_2. When the calcination temperature of doped TiO_2 increases to 700°C the photo-catalytic reaction rate tends to increase and then decreases at higher calcination temperature, because at high calcination temperature samples have a rutile structure and give lower degradation efficiency compared with the samples calcined at lower temperatures. Our results are in good agreement with those obtained in a previous study. On the basis of our previous results, a nanocomposite of two phases of the same semiconductor and good crystallization of anatase both lead to an improvement in photo-activity. Thus, the sample calcined at 700°C has higher crystallization and intensity of anatase phase due to the photocatalytic activity increase [29].

3.4 SEM-EDX and TEM Analysis of Pure and Doped TiO_2 nanopowders

Figure 7 shows the surface morphology of the pure and doped TiO_2 nanoparticles at temperature 500°C. Figure 7b presents the images of doped TiO_2 nanoparticles which illustrate the small size (100-200 nm) of the undoped particle. This result confirms that the width of the anatase peak diffraction from XRD indicates the smaller crystalline size at 500°C (Fig. 1). In addition to SEM analysis, EDX analysis was performed on powders in order to investigate the chemical structure. The analyses revealed the existence of Ti as the main element. The EDX data of doped TiO_2 in Fig. 8 shows two peaks around 4.5 keV. The intense peaks is assigned to the bulk TiO_2 and the less intense one to the surface TiO_2. The peaks of Cu are distinct in Fig. 8 at 0-2.6 keV. The less intense peak is assigned to dopant in the TiO_2 lattices. These results confirm the existence of cations in the solid catalysts.

The particle size and shape of pure and doped TiO_2 nanoparticles calcined at a temperature of 500°C were investigated by TEM and are shown in Fig. 9. The TEM images illustrate that almost all of the particles are of spherical shape and the effect of doping on particle size is considerable. A decrease of particle size with doping of Cu is attributed to inhibition of the crystal growth. The TEM results are in good agreement with XRD data measured using Scherrer's equation and surface area data as presented in Table 1.

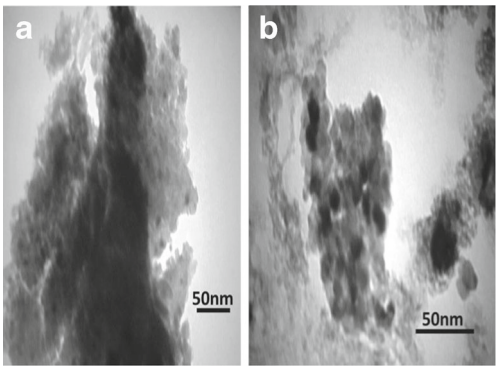

Fig. 9 TEM micrograph of T,TC calcined at 500 °C **a)** T, **b)** TC

4 Conclusion

This study focused on the effects of calcination temperature and Cu dopant on phase transformation, crystallite size, and photo-catalytic activity of titania nanopowders. It was shown that the crystal phases and crystallite sizes of doped TiO_2 nanopowders. largely depend on the calcinations temperature. Crystalline anatase single phase was found at a calcinations temperature range of 500–700°C and rutile phase was formed at a temperature of 800–1000°C. The photo-catalytic activity of the doped nanopowders is higher than that of pure TiO_2 nanopowders. Cu^{2+} substitution for Ti^{4+} in the TiO_2 lattice results in a decrease in the rate of photo-generated electron–hole recombination that is responsible for the enhancement in the photo-catalytic degradation rate.

References

1. Gopal M, Chan W, Jonghe L (1997) J Mater Sci 32:6001–6008
2. Mark HF, Othmer DF, Overberger CG, Seaberg GT (eds) (1983), vol 23. Wiley, New York
3. Weast RC (1984) Handbook of chemistry and physics. CRC Press, Boca Raton, pp B–154
4. Kostov I (1973) Minerology, 3rd edn. Nauka, Izkustia, Sofia
5. Yang SW, Gao L (2005) J Am Ceram Soc 88:968–970
6. Karakitsou KE, Verykios XE (1993) J Phys Chem B 97:1184–1189
7. Hu C, Lan Y, Hu X, Wang A (2006) J Phys Chem B 110:4066–4072
8. Sakatani Y, Grosso D, Nicole L, Boissiere C, Illia S, Sanchez C (2007) J Mater Chem 16:77–82

9. Fujishima A, Rao TN, Tryk DA (2001) J Photochem Photobiol C:Photochem Rev 1:1–21
10. Parkin IP, Palgrave RG (2005) J Mater Chem 15:1689–1695
11. Mills A, Lee SK (2006) J Photochem Photobiol A Chem 182:181–186
12. Zanderna AW, Rao CNR, Honig JM (1958) Trans Faraday Soc 54:1069–1073
13. Li FB, Li XZ, Hou MF, Cheah KW, Choy WCH (2005) Appl Catal A General 285:181–189
14. Kubacka A, Fuerte A, Martinez-Arias A, Fernandez-Garcia M (2007) Appl Catal B Environ 74:26–33
15. Jin Z, Zhang X, Li Y, Li S, Lu G (2007) Catal Commun 8:1267–1273
16. Sayilkan HI (2007) Appl Catal A General 319:230–236
17. Xie Y, Yuan C (2004) Appl Surf Sci 221:17–24
18. Bouras P, Slathatos E, Lianos P (2007) Appl Catal B Environ 73:51–59
19. Kudo A (2007) Int J Hydrogen Energy 32:2673–2678
20. Ihara T, Miyoshi M, Ando M, Sugihara S, Iriyama Y (2001) J Mater Sci 36:4201–4207
21. Ihara T, Miyoshi M, Iriyana Y, Matsumoto O, Sugihara S (2003) Appl Catal B Environ 42:403–409
22. Prokes SM, Gole JL, Chen X, Burda C, Carlos WE (2005) Adv Funct Mater 15:161–167
23. Najibi Ilkhechi N, Koozegar Kaleji B (2014) J Sol-Gel Sci Technol 69:351–356
24. Balachandran K, Venckatesh R, Sivraj R (2010) Int J Eng Sci Technol 28:3695–3700
25. Hussain ST, Mazhar M, Siddiqa A, Javid H, Siddiq M (2012) Catalysis J 5:21–30
26. Jin Z, Zhang X, Li Y, Li S, Lu G (2007) Catal Commun 8:1267–1273
27. Salavati-Niasari M, Davar F, Mir N (2008) Polyhedron 27:3514–3518
28. Kapusuz D, Park J (2013) Ozturk A 74:1026–1031
29. Najibi Ilkhechi N, Koozegar Kaleji B, Fallah D J Opt Quant Electron. doi:10.1007/s11082-014-9940-0
30. Lia XZ, Li FB, Yang CL, Ge WK (2001) J Photochem Photobiol A 141:209–217
31. Li XZ, Li FB (2001) Environ Sci Technol 35:2381–2387